

GCond: Gradient Conflict Resolution via Accumulation-based Stabilization for Large-Scale Multi-Task Learning

Evgeny Alves Limarenko and Anastasiia Alexandrovna Studenikina

Moscow Institute of Physics and Technology, Dolgoprudny, Moscow Region, Russia

Corresponding author:
Evgeny Alves Limarenko

Email address: e@alevlab.com

ABSTRACT

Preprint. Under review.

In multi-task learning (MTL), gradient conflict poses a significant challenge. Effective methods for addressing this problem, including PCGrad, CAGrad, and GradNorm, in their original implementations are computationally demanding, which significantly limits their application in modern large models and transformers. We propose Gradient Conductor (GCond), a method that builds upon PCGrad principles by combining them with gradient accumulation and an adaptive arbitration mechanism. We evaluated GCond on self-supervised learning tasks using MobileNetV3-Small and ConvNeXt architectures on the ImageNet 1K dataset and a combined head and neck CT scan dataset, comparing the proposed method against baseline linear combinations and state-of-the-art gradient conflict resolution methods. The stochastic mode of GCond achieved a two-fold computational speedup while maintaining optimization quality, and demonstrated superior performance across all evaluated metrics, achieving lower L1 and SSIM losses compared to other methods on both datasets. GCond exhibited high scalability, being successfully applied to both compact models (MobileNetV3-Small) and large architectures (ConvNeXt-tiny and ConvNeXt-Base). It also showed compatibility with modern optimizers such as AdamW and Lion/LARS. Therefore, GCond offers a scalable and efficient solution to the problem of gradient conflicts in multi-task learning.

Keywords: Deep learning, Multi-task learning, Gradient accumulation, Gradient conflicts, PCGrad, Computed tomography

INTRODUCTION

Multitask learning (MTL) enables neural networks to simultaneously optimize multiple related objective functions, which enhances generalization and computational efficiency compared to training separate models Kendall et al. (2018). MTL can be viewed as a multi-criteria optimization problem that seeks to find an optimal solution in the space of trade-offs between multiple competing objectives under resource constraints Sener and Koltun (2018). It is important to distinguish between two types of multi-objective learning: classical multi-task learning with multiple tasks, such as simultaneous image classification and segmentation, and multi-objective optimization of a single task using a combination of multiple loss functions. The latter approach can be considered as a special case of multi-criteria optimization, where a single task is optimized through multiple quality metrics, for example, a combination of L1 and SSIM for image reconstruction Lin et al. (2019); Rosenfeld and Tsotsos (2018). One of the key factors influencing optimization dynamics is batch size. It determines the number of dataset elements processed in one iteration of the training process and has a substantial impact on model performance Peng et al. (2018). Modern research demonstrates that increasing batch size reduces model training time. In particular, a study by Jia and colleagues showed the possibility of reducing ResNet-50 training time on ImageNet from 29 hours to several minutes when increasing batch size from 256 to 64K Jia et al. (2018). Furthermore, the combination of high image resolution with large batch size demonstrates an average increase of 22%

in accuracy for image classification and segmentation models Piao et al. (2023). However, practical application of large batches is limited by available GPU memory. Modern complex deep learning models require substantial amounts of memory for parameter storage, which significantly restricts the batch sizes that can be accommodated in device memory You et al. (2020). Exceeding the available memory necessitates reducing image resolution or decreasing batch size, which negatively affects final model quality Piao et al. (2023). Gradient accumulation methods offer an elegant solution to the limited memory problem while preserving the efficiency of large batches. This approach divides a large batch into K smaller micro-batches, which are processed sequentially with accumulation of computed gradients without exceeding the device memory limit Kim et al. (2024). After accumulating gradients across all micro-batches, they are averaged to approximate the full batch gradient and the optimizer performs parameter updates. Mathematically, the gradient obtained through gradient accumulation is equivalent to the gradient computed for a large batch, ensuring the method’s theoretical validity Liu et al. (2025). Although gradient accumulation increases training time due to replacing parallel computations with sequential ones, it is widely used in MTL tasks as it helps reduce the variance of the accumulated gradients Smith et al. (2017). A fundamental challenge in practical MTL implementation is accompanied by the fundamental problem of gradient conflicts, when gradients from different loss functions are directed in opposite directions, which manifests as negative cosine similarity between task gradients, and leads to mutual suppression of parameter updates Yu et al. (2020). This is accompanied by slower convergence, loss of important details, and suboptimal solutions. This effect is particularly pronounced in early training stages, when model parameters have not yet adapted to the multi-objective optimization landscape, which can cause loss of important details and deterioration of solution quality Golnari and Diba (2025). Experiments have confirmed that direct averaging of conflicting gradients leads to gradient bias, which can significantly worsen performance of individual tasks, since parameter updates become biased toward dominant tasks Chen et al. (2020); Liu et al. (2023); Mang et al. (2024). The problem is exacerbated by the “tragic triad,” when conflicting gradient directions combine with significant differences in magnitude and high curvature in the optimization landscape Zhang et al. (2024). Under such conditions, traditional approaches demonstrate critical performance degradation compared to separate task training Shi et al. (2023). Modern approaches to gradient conflict resolution fall into three categories: naive summation Fifty et al. (2021), task balancing methods such as GradNorm Chen et al. (2018), and projection methods such as PCGrad Yu et al. (2020) and CAGrad Liu et al. (2021). Naive summation methods are based on joint task training with averaged loss functions and often with equal weights Fifty et al. (2021). However, as shown in research, direct gradient averaging often worsens results compared to separate task training Zhang et al. (2024). Task balancing approaches such as GradNorm dynamically adjust loss function weights to equalize their gradient magnitudes, but do not solve the direction problem, since under this approach even gradients with identical norms can be directed in opposite directions, creating conflict Sun et al. (2025). The most promising are considered to be projection methods or Gradient Surgery methods, among which Projecting Conflicting Gradients (PCGrad) has become the de facto standard. PCGrad addresses conflicts by iterating through pairs of task gradients. For each conflicting pair, it projects one gradient onto the orthogonal complement of the other. The selection of which gradient to project is determined by their fixed order in the iteration, the effects of which are mitigated by randomly shuffling the task order at each training step Yu et al. (2020). Conflict-Alleviated Gradient Descent (CAGrad) developed this idea, proposing the search for a common update direction by modifying gradients, transforming obtuse angles between them into acute ones and minimizing the average loss function Liu et al. (2021). PCGrad and CAGrad have been successfully used repeatedly in various computer vision tasks, including several medical imaging tasks Wu et al. (2023); El Nahhas et al. (2024). These methods have several significant limitations: they work on noisy gradients from single mini-batches and require substantial computational resources. Moreover, in their original implementation, PCGrad and CAGrad require significant memory costs due to the need to preserve computational graphs of weights between iterations, making them inapplicable in their original implementation for modern architectures like Transformer or ConvNeXt with large effective batch sizes Lau et al. (2024). More modern projection methods for gradient conflict resolution such as Aligned-MTL, using object-level gradients instead of parameter-level gradients, or Similarity-Aware Momentum Gradient Surgery, dynamically adapting the gradient descent optimization process based on task gradient magnitude similarity, significantly reduce computational costs and accelerate training Senushkin et al. (2023); Borsani et al. (2025). However, to demonstrate their effectiveness, these methods rely on synthetic data, where artificial MTL tasks with controlled optimization conditions are used Navon

et al. (2022). Such an approach may prove unviable when working with real medical data, characterized by high dimensionality, noise, data incompleteness, and complex nonlinear dependencies between tasks. In this work, we propose Gradient Conductor (GCond) - a method that builds upon the ideas of PCGrad by combining them with gradient accumulation. Unlike reactive strategies that eliminate conflicts at each step, GCond implements a two-phase "accumulate-then-resolve" process: during the accumulation phase, averaged gradients with low variance are computed. Then during the arbitration phase, an adaptive conflict resolution mechanism is applied, significantly improving the precision of gradient adjustments while reducing computational requirements. The contribution of our work can be described as follows:

1. We apply a novel approach to gradient conflict resolution based on accumulation, to reduce gradient variance before conflict resolution, which enhances stability and reliability of corrections.
2. We introduce an adaptive multi-zone arbitration mechanism with continuous conflict resolution strategies, which are based on learning dynamics (stability, strength, domination), for decision making.
3. Our approach demonstrates high scalability, performance, and efficiency on both single-channel medical imaging data and color natural images.

METHODS

Accumulation as Variance Reduction

The proposed GCond method organically integrates its gradient conflict resolution mechanism-projecting conflicting gradients onto each other, similar to PCGrad-with gradient accumulation. Specifically, instead of operating on "noisy" gradients $g(\theta; b)$ from individual mini-batches, which are unbiased but high-variance estimates of the true gradient $G(\theta)$, GCond utilizes accumulated gradients. GCond addresses this problem through a two-phase approach: accumulation and arbitration. In the first phase (Estimation Phase), over K steps, gradients for each of the N loss functions are computed on different mini-batches and accumulated in N independent accumulator buffers. This is followed by the Resolution Phase: after K steps, the proposed adaptive arbitrator mechanism is applied to the N accumulated, averaged gradients to resolve conflicts and produce a single, unified gradient, which is then passed to the optimizer. GCond uses gradient accumulation to obtain averaged gradients over K steps:

$$\hat{g}_i = \frac{1}{K} \sum_{k=1}^K g_i(\theta; b_k)$$

where \hat{g}_i is the accumulated gradient for task i , K is the number of accumulation steps. Consequently, the variance of the accumulated gradients is significantly reduced:

$$\text{Var}(\hat{g}_i) = \frac{1}{K} \text{Var}(g_i)$$

This provides more stable and reliable estimates of the true gradient directions, enabling precise detection and resolution of conflicts (assuming independent or weakly correlated micro-batches). Thus, GCond employs a standard gradient accumulation mechanism to suppress noise, which fundamentally distinguishes it from other methods. This transforms the conflict resolution procedure into a more robust analysis of the true descent directions of the loss functions. Such an approach turns metrics of inter-gradient interactions, like the cosine similarity between accumulated gradients \hat{g}_i and \hat{g}_j , from high-variance random variables into statistically reliable indicators of the true conflict between tasks. This ensures more informed and stable gradient correction decisions.

Adaptive Multi-Zone Arbitration

After obtaining the accumulated gradients $\{\hat{g}_1, \dots, \hat{g}_n\}$, our arbitration mechanism resolves conflicts iteratively, starting with the most severe ones. At each iteration, the pair of gradients (\hat{g}_i, \hat{g}_j) with the minimum cosine similarity is identified:

$$c = \cos(\hat{g}_i, \hat{g}_j) = \frac{\hat{g}_i \cdot \hat{g}_j}{\|\hat{g}_i\| \|\hat{g}_j\|}$$

Instead of discretely switching between resolution strategies, our approach employs a continuous modulation governed by a piecewise function. This function non-linearly maps the cosine similarity $c \in [-1, 1]$ to an effective conflict angle $\alpha_{\text{eff}} \in [0, \pi]$, guided by three thresholds: θ_{weak} , θ_{main} , and θ_{crit} .

$$\alpha_{\text{eff}}(c) = \begin{cases} \pi & \text{if } c \leq \theta_{\text{crit}} \\ \frac{\pi}{2} + \frac{\pi}{2} \left(\frac{c - \theta_{\text{main}}}{\theta_{\text{crit}} - \theta_{\text{main}}} \right)^p & \text{if } \theta_{\text{crit}} < c < \theta_{\text{main}} \\ \frac{\pi}{2} \left(1 - \frac{c - \theta_{\text{main}}}{\theta_{\text{weak}} - \theta_{\text{main}}} \right) & \text{if } \theta_{\text{main}} \leq c < \theta_{\text{weak}} \end{cases}$$

Here, p is a hyperparameter (`remap_power`) controlling the mapping’s curvature. The projection strengths for the winner (g_w) and loser (g_l) gradients are then determined by two trigonometric modulators derived from this angle: a winner scaling factor

$$s_w = \sin(\alpha_{\text{eff}})$$

and a loser scaling factor

$$s_l = \sin(\min\{\alpha_{\text{eff}}, \pi/2\})$$

This mechanism ensures smooth, continuous transitions between conflict resolution behaviors, which are detailed in Table 1. Conflicts where $c \geq \theta_{\text{weak}}$ are considered agreement, and no correction is applied.

Conflict Zone	Condition	Resolution Strategy
Agreement	$c \geq \theta_{\text{weak}}$	No correction. The arbitration loop terminates.
Mild Conflict	$\theta_{\text{main}} \leq c < \theta_{\text{weak}}$	Symmetric Scaled Projection. α_{eff} maps to $(0, \pi/2]$. Both scaling factors, s_w and s_l , decay from 1 to 0. Projections are applied symmetrically, with their magnitude diminishing as c approaches θ_{weak} .
Moderate Conflict	$\theta_{\text{crit}} \leq c < \theta_{\text{main}}$	Asymmetric Projection. α_{eff} maps to $(\pi/2, \pi]$. The loser is fully projected ($s_l = 1$). The winner receives a partial corrective projection that starts at zero and strengthens as c approaches θ_{main} (s_w grows from 0 to 1).
Critical Conflict	$c < \theta_{\text{crit}}$	Winner preservation. α_{eff} is fixed at π . The winner’s gradient is unchanged ($s_w = 0$), while the loser is fully projected onto the winner’s orthogonal complement ($s_l = 1$).

Table 1. Zonal Classification of Gradient Conflicts.

The method for identifying the “winner” and “loser” in conflicting pairs is described in the following section.

Winner Selection

In situations requiring arbitration (i.e., in moderate and critical conflict zones where $c < \theta_{\text{weak}}$), we identify a “winner” gradient using a weighted score:

$$\text{Score}_i = w_{\text{stability}} \cdot \max(0, S_i) + w_{\text{strength}} \cdot N_i$$

where: S_i (Stability): Represents the cosine similarity between the current accumulated gradient and the gradient from the previous optimization step:

$$S_i = \cos(\hat{g}_i(t), \hat{g}_i(t-1))$$

Stability rewards gradients that maintain their direction, leading to a smoother training trajectory. N_i (Strength): A relative measure of a gradient’s magnitude. It is calculated by first normalizing the gradient’s norm by its Exponential Moving Average (EMA), and then scaling this value by the sum of the scaled norms for both conflicting gradients:

$$N_i = \frac{\|\hat{g}_i\|_2 / (\text{EMA}(\|\hat{g}_i\|_2) + \epsilon)}{\sum_{k=i,j} \|\hat{g}_k\|_2 / (\text{EMA}(\|\hat{g}_k\|_2) + \epsilon)}$$

where strength prioritizes gradients that are momentarily stronger relative to their historical average and relative to their current competitor. This allows for a rapid response to tasks that suddenly become more important. Additionally, a dominance prevention mechanism is implemented: if the same task wins conflicts for a specified number of iterations (`dominance_window`), its opponent is automatically designated the winner. This prevents the training of other tasks from stagnating.

Experimental Settings

Computational Environment Experiments with simpler models were conducted on a system with an NVIDIA RTX 4080 GPU (16 GB VRAM) and a 20 core Intel(R) Core(TM) Ultra 7 265K CPU. The software environment included PyTorch 2.7.0, Python 3.12.3, Ubuntu 24.04, and CUDA 12.8. Final testing on the complex ConvNeXtV2-Base model was performed on a system with an NVIDIA H200 GPU (140 GB VRAM) and a 48-core Intel(R) XEON® PLATINUM 8568Y+ CPU. Its software environment included PyTorch 2.5.1, Python 3.10.18, Ubuntu 22.04, and CUDA 12.4.

Experimental Datasets To ensure fair and reproducible comparisons, all experiments were conducted under strictly controlled conditions. We implemented a self-supervised image reconstruction task (Masked Image Modeling) on a large dataset of medical head and neck CT scans from three public datasets: RSNA Intracranial Hemorrhage Detection Flanders et al. (2020), RSNA Cervical Spine Fracture Detection Lin et al. (2023), and RADCIURE from The Cancer Imaging Archive (TCIA) Welch et al. (2023), containing 2,199,444 DICOM (Digital Imaging and Communications in Medicine) files. All experiments used a fixed patient-based data split to ensure reproducibility and fair method comparison. Additionally, the performance of the proposed GCond model was verified on benjamin-paine/imagenet-1k-256x256-a version of the ILSVRC 2012 (ImageNet) dataset containing 1.28 million training images and 50,000 validation images.

Evaluation Indicators Model quality was assessed using L1 Loss and SSIM Loss on the validation set. Efficiency was evaluated based on peak VRAM consumption (MB) and throughput (samples/sec). Stability was monitored through gradient norms and loss curve dynamics.

Experimental Configuration In our experiments, we used a Masked Autoencoder (MAE) architecture with a MobileNetV3-Small encoder and a 2 layer Transformer decoder (embedding dimension 256). For scalability analysis, a ConvNeXt-tiny architecture was used. All models were trained for 15 epochs with a linear warmup for 2 epochs, followed by a cosine learning rate decay. We used the AdamW optimizer with a learning rate of 2.0×10^{-4} and a weight decay of 0.05. A large effective batch size of $256 \times 24 = 6144$ was used for training stability and to reduce gradient variance. Input images were preprocessed by center cropping and resizing to a resolution of 256×256 pixels. Two loss functions, calculated on the masked patches, were used: L1 loss to enforce pixel-level accuracy ($\lambda_{L1} = 0.85$) and SSIM loss to promote structural similarity ($\lambda_{SSIM} = 0.15$). A key aspect of our experimental design was the deliberate separation of the value spaces for these two metrics. The L1 loss was calculated directly in the z-normalized space, whereas the SSIM loss was computed in the standard pixel-value range of $[0, 1]$ after applying an inverse normalization to both the model’s predictions and the target patches. This approach was chosen specifically to exacerbate the natural conflict between the pixel-wise L1 metric and the perceptual SSIM metric, thereby creating a more demanding test scenario for evaluating the effectiveness of gradient conflict resolution strategies. We benchmarked the proposed GCond algorithm against a Baseline (standard weighted gradient summation) and state-of-the-art methods: PCGrad, CAGrad, and GradNorm, implemented from their respective papers.

Hyperparameter Analysis A comprehensive ablation study of key hyperparameters was conducted to determine the optimal configuration for the GCond module. A systematic grid search on the CT image dataset with the combined L1 and SSIM loss function identified the most robust configuration, providing an effective balance between stability and convergence speed. Specifically, the optimal arbitration weights were `tie_breaking_weights = (0.8, 0.2)`, which prioritize gradient direction stability over its instantaneous magnitude. The optimal three-zone conflict threshold system was `conflict_thresholds = (-0.8, -0.5, 0)`, which clearly delineates the intervention modes.

Core Parameters. We recommend fixing `remap_power = 2` in combination with the `use_smooth_logic=True` option. This configuration introduces a quadratic non-linearity into the `_get_effective_alpha` function, ensuring smoother gradient modulation in the weak conflict

zone ($\cos(\theta) \rightarrow \theta_{\text{weak}}$) and more decisive correction as the conflict intensifies (as $\cos(\theta) \rightarrow \theta_{\text{crit}}$), thereby stabilizing training dynamics.

Threshold Values. The threshold configuration of $(-0.8, -0.5, 0.0)$ demonstrated the best long-term convergence. A value of $\theta_{\text{weak}} = 0.0$ serves as an intuitive boundary between conflict and agreement. The lower threshold $\theta_{\text{crit}} = -0.8$ activates asymmetric conflict resolution only when vectors are significantly anti-parallel, preventing overly aggressive correction for moderate disagreements. Notably, in the early training stages (epochs 2-5), the configuration $\theta = (-1.0, -0.4, 0.1)$ yielded faster results. Here, $\theta_{\text{weak}} = 0.1$ treated even slight agreement as a conflict, subjecting the gradients to symmetric orthogonalization. This accelerated the initial direction finding but later restricted exploration of the parameter space, leading to stagnation in a local optimum.

Arbitration Weights. For `tie_breaking_weights`, an imbalance proved preferable to equilibrium. It allows the arbiter to consistently adhere to one strategy (gradient stability or relative strength), avoiding oscillations in decision-making when resolving critical conflicts.

Momentum. The `momentum_beta` parameter showed optimal results in the range around 0.9, consistent with common practices for adaptive optimizers.

Dominance Window. Our ablation study on the `dominance_window (w)` hyperparameter revealed that $w=3$ and $w=0$ (disabled) yielded the top results. However, the dominance mechanism is stateful, making the gradient update dependent on the optimization history. To ensure a fair and stateless comparison across methods, thereby isolating their intrinsic properties, we set $w=0$ for all primary experiments. While this guarantees reproducibility and a controlled evaluation, we acknowledge that a non-zero window could be optimal in practical applications to prevent task starvation. The charts can be accessed in the supplementary materials section. Despite the presence of numerous hyperparameters, our analysis showed that the proposed set of default values, initially selected for medical segmentation tasks, demonstrates a high degree of versatility and ensures stable convergence across diverse datasets, including ImageNet.

RESULTS

Performance Analysis of the Stochastic GCond Mode

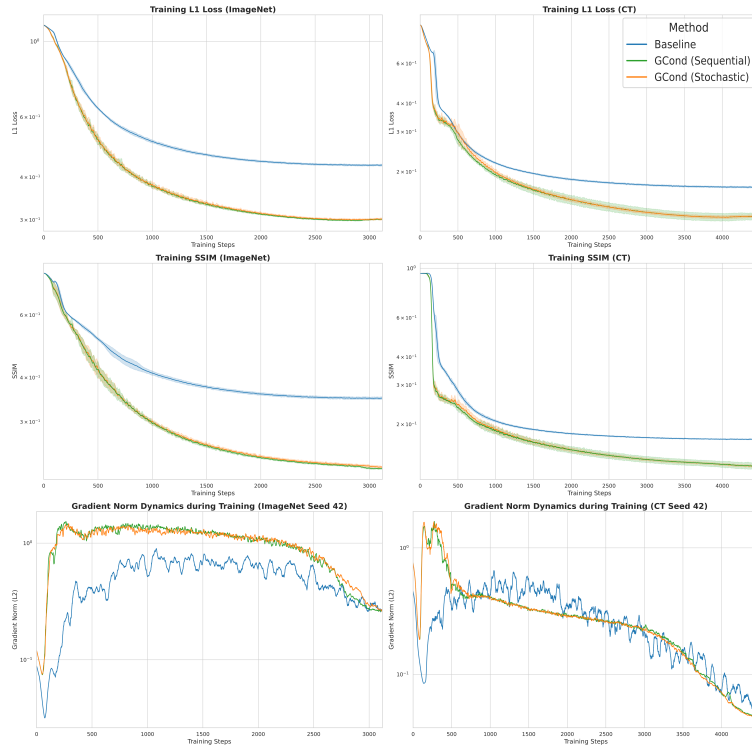


Figure 1. Comparison of convergence for L1 and SSIM losses, and L2-norms of gradients for the stochastic and exact GCond modes on both datasets during MobileNetV3-Small model training

To enhance computational efficiency, especially with a large number of accumulation steps ($K \gg 1$), a stochastic mode for GCond was developed. In this mode, the K accumulation steps are divided into N non-overlapping blocks of K/N steps for each loss function. The gradient for each task i is accumulated over its unique sequence of mini-batches. It is important to note that all gradients g_i are computed with respect to the same model weight state θ_t , ensuring that the final accumulated gradients \hat{g}_i are unbiased and comparable. This approach not only reduces computational costs, but also promotes more robust gradient estimates by analyzing data from different samples. A comparison of the training dynamics between the stochastic and the exact (sequential) modes is presented in Fig. 1. The results demonstrate that the differences between the learning curves are statistically insignificant. This confirms the hypothesis that with a sufficiently large effective batch size (in this case, $256 \times 24 = 6144$), a sparse sampling of gradients allows for the formation of a statistically reliable estimate for conflict resolution. The stochastic mode was twice as computationally efficient as the exact (sequential) mode while maintaining training quality. The validation curves Fig. 2 confirms these observations.

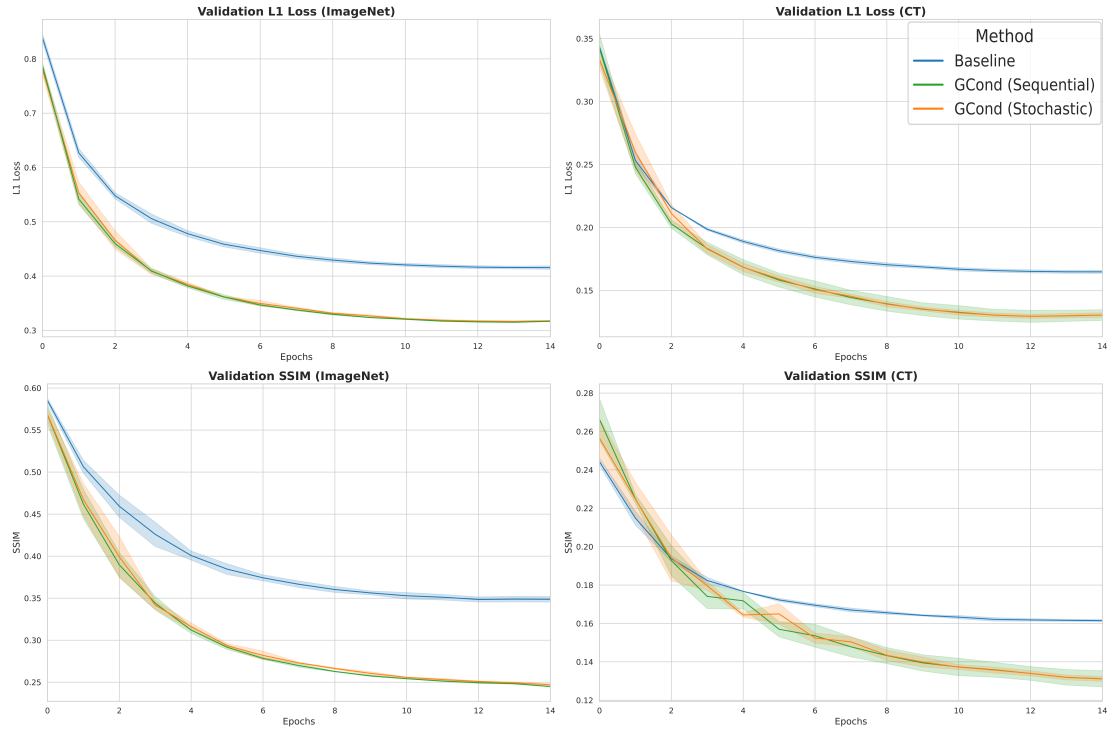


Figure 2. Validation of L1 and SSIM loss functions for the stochastic and exact GCond modes on both datasets during MobileNetV3-Small model training

Comparative Analysis of Optimization Quality

To evaluate the effectiveness of the proposed GCond method, a comparison was conducted against state-of-the-art gradient conflict resolution approaches (PCGrad, CAGrad, GradNorm) and a baseline linear combination of loss functions (Baseline). Table 2 presents the final validation metrics, L1 Loss and Structural Similarity Index (SSIM), for the MobileNetV3-Small model on the ImageNet and CT HN datasets.

The results demonstrate the consistent superiority of GCond over both the baseline and other conflict resolution methods across both datasets. Notably, the projection-based methods, PCGrad and CAGrad, performed worse than the baseline. A key finding is the statistical equivalence between the sequential and stochastic GCond modes. Their mean performance metrics are nearly identical, with significantly overlapping confidence intervals suggesting no statistically significant difference. This result strongly justifies using the more computationally efficient stochastic mode. Consequently, all subsequent experiments were conducted using the stochastic GCond mode.

Method	ImageNet		CT HN	
	L1	SSIM	L1	SSIM
Baseline	0.41542 ± 0.00716	0.34845 ± 0.00764	0.16473 ± 0.00307	0.16145 ± 0.00154
CAGrad	0.42263 ± 0.00323	0.32793 ± 0.00643	0.17779 ± 0.00485	0.16096 ± 0.00222
GradNorm	0.41635 ± 0.00204	0.31818 ± 0.00579	0.16847 ± 0.00496	0.15930 ± 0.00241
PCGrad	0.42324 ± 0.00270	0.34221 ± 0.00462	0.17311 ± 0.00683	0.16286 ± 0.00371
GCond (Sequential)	0.31493 ± 0.00056	0.24485 ± 0.00093	0.12942 ± 0.01195	0.13118 ± 0.01049
GCond (Stochastic)	0.31655 ± 0.00287	0.24704 ± 0.00262	0.12941 ± 0.00405	0.13111 ± 0.00315

Table 2. Best validation metrics for the MobileNetV3-Small model.

Analysis of Training Process Dynamics

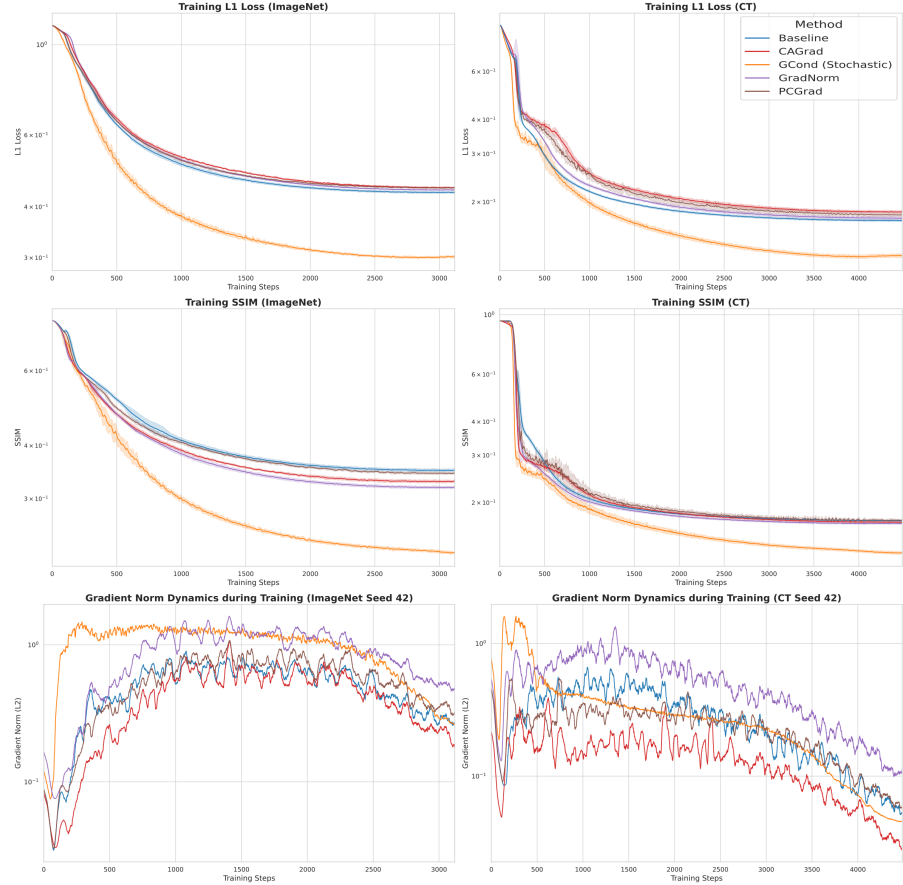


Figure 3. Comparison of the dynamics of L1 and SSIM loss functions, and L2-norms of gradients for all methods on both datasets during MobileNetV3-Small model training

Fig. 3 illustrates the dynamics of the loss functions and the L2-norms of gradients during training on the CT HN and ImageNet datasets, respectively. Across all loss plots, it is observed that simple task weighting (Baseline) yields more stable and smoother training trajectories compared to traditional gradient conflict resolution methods. On both datasets, PCGrad, GradNorm, and CAGrad consistently underperformed the baseline in terms of L1 loss. Regarding the SSIM loss on the ImageNet dataset, although PCGrad, GradNorm, and CAGrad showed better results than the baseline, their training curves were accompanied by noticeable high-frequency oscillations and earlier stagnation on a plateau. In contrast, the stochastic mode of GCond demonstrates a clear superiority over all compared methods. The dynamics of the L1 and SSIM loss functions during training directly correspond to the dynamics of the gradient L2-norms. It is evident that GradNorm and PCGrad produce significant sawtooth-like oscillations in amplitude, while CAGrad systematically suppresses the gradient norm, especially on the

CT HN dataset, which is equivalent to an excessively small effective learning step. The reasons for this lie in the nature of these algorithms, as they primarily focus on handling mini-batch gradients that are often sharply anisotropic. Against this backdrop, the simple summed gradient of the Baseline remains an unbiased, low-variance estimate of the descent direction and thus proves to be more reliable. The proposed GCond mechanism exhibits more monotonic and less noisy behavior because destructive projections are mitigated smoothly, and the step direction is statistically justified and largely invariant to the scale of the layers. The key factor is the precise choice of direction: GCond aggregates gradients over a large effective batch and, through arbitration, forms a globally consistent update vector. Its normalization and EMA-smoothing stabilize the step magnitude, allowing the Adam optimizer to perform larger and more reliable updates in the chosen direction.

These conclusions are further illustrated by the validation curves Fig. 4. The trajectories of the stochastic GCond mode are consistently below the curves of the other methods, from the early epochs to the final plateau. This gap is maintained with less variance between epochs, confirming the proposed approach’s ability to provide a more stable, conflict-resilient estimate of the optimization step.

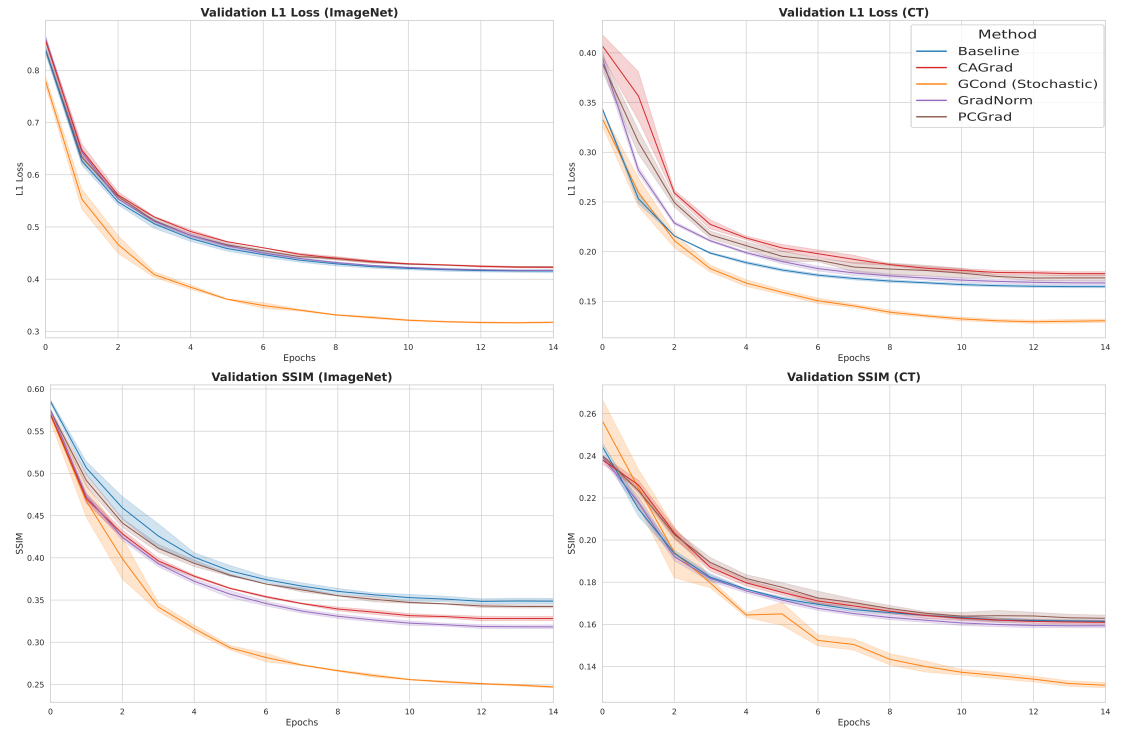


Figure 4. Validation of L1 and SSIM loss functions for all methods on both datasets during MobileNetV3-Small model training

Analysis of Computational Efficiency

To ensure a fair comparison, the number of accumulation steps was fixed across all experiments, and for each implementation, only the batch size was increased to fill 16 GB of VRAM. This maintains an equal number of updates per epoch and allows for a correct comparison of method throughput. The GCond implementation is based on `torch.func.functional_call` with an explicit call to `autograd.grad` on “fresh” leaf parameters: the gradients for each task are computed independently, immediately accumulated into bf16 buffers, and the computation graph is released. This approach eliminates the need to retain a common graph until the last task (`retain_graph=True` in classic PCGrad/CAGrad/GradNorm), meaning GCond’s peak memory consumption is close to that of a single backward pass plus a fixed overhead for the accumulation buffers. This explains the slightly higher VRAM usage on the small MobileNetV3-Small model Table 3.

On the ConvNeXt-Base architecture with 16 GB of VRAM, the PCGrad and CAGrad methods failed to run even with a batch size of 1. This was due to the necessity of retaining the computation graph and

Method	ImageNet			CT HN		
	GPU Memory (MB)	Epoch Time (s)	Throughput (samples/s)	GPU Memory (MB)	Epoch Time (s)	Throughput (samples/s)
Baseline	6888.98 \pm 0.00	901.15 \pm 1.27	1421.73 \pm 1.99	4257.19 \pm 0.00	778.09 \pm 5.95	2367.52 \pm 16.44
CAGrad	7514.00 \pm 0.00	965.23 \pm 0.47	1327.33 \pm 0.65	4682.19 \pm 0.00	989.17 \pm 1.39	1861.28 \pm 2.59
GradNorm	7056.58 \pm 0.00	965.25 \pm 0.55	1327.29 \pm 0.75	4319.14 \pm 0.00	993.34 \pm 2.04	1853.50 \pm 3.76
PCGrad	7515.89 \pm 0.27	968.59 \pm 0.74	1322.73 \pm 1.00	4679.83 \pm 0.00	993.24 \pm 2.47	1853.72 \pm 4.54
GCond	8739.54 \pm 0.76	905.10 \pm 2.96	1415.66 \pm 4.63	4856.77 \pm 0.00	822.87 \pm 3.56	2237.83 \pm 9.52

Table 3. Comparative performance of methods on the MobileNetV3-Small model.

individual gradient vectors, as the memory consumption of these methods scales linearly with the number of tasks. In contrast, GCond was able to process up to 70 images thanks to its graph-free task processing. Therefore, the ConvNeXt-Tiny model was used to compare the speed of the algorithms Table 4. With a fixed number of accumulation steps, GCond achieves baseline throughput and surpasses PCGrad/CAGrad in performance (throughput) with comparable memory consumption (VRAM). Thus, a key advantage of GCond is its scalability.

Method	Batch Size	Effective Batch Size	GPU Memory (MB)	Epoch Time (s)	Throughput (samples/s)
PCGrad	96	2304	14192.53	4817.08	382.20
CAGrad	96	2304	14181.52	4872.46	377.85
GradNorm	148	3552	13958.67	4992.46	368.77
Baseline	170	4080	14510.72	3198.98	575.52
GCond	162	3888	14540.23	3205.20	574.40

Table 4. Comparative performance of methods on the ConvNeXt-Tiny model, CT HN dataset Seed 42.

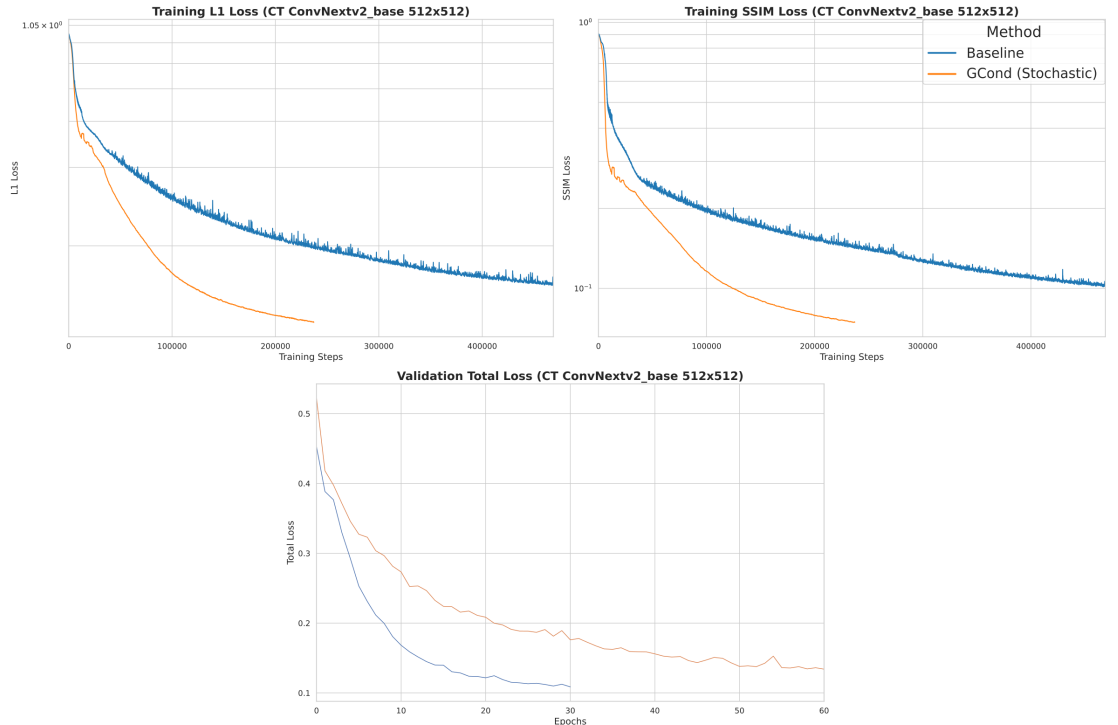


Figure 5. Comparison of training quality between GCond and Baseline on the CT dataset using the ConvNeXtV2-Base mode

Additionally, experiments with the ConvNeXtV2-Base architecture on a SSL task with L1 and SSIM losses on the CT HN dataset with 512×512 resolution images demonstrated significant improvements in convergence and stability. With the GCond model, the L1 and SSIM training curves were characterized by substantially greater smoothness and lower variance compared to the Baseline. On the validation set, by the 15th epoch (10 of which were a warmup period), GCond had already reached and subsequently

surpassed the final performance level of the Baseline model trained for 60 epochs. When training was stopped at the 30th epoch, a noticeable gap in both loss functions persisted Fig.5. We intentionally limited GCond’s training to 30 epochs, as the goal of this experiment was to demonstrate the method’s potential efficiency—that is, GCond achieves lower loss values in the same or fewer epochs.

Monitoring the activations of the final encoder layer revealed a nearly twofold expansion in the distribution of activations from the very first epochs. We interpret this as an indicator of a richer, non-collapsing representation and a consequence of the high signal-to-noise ratio in the gradient and the conflict-resilient projection in GCond, which enhances both optimization speed and the model’s potential generalization capability. A detailed analysis of the large model’s representations is a subject for our future work.

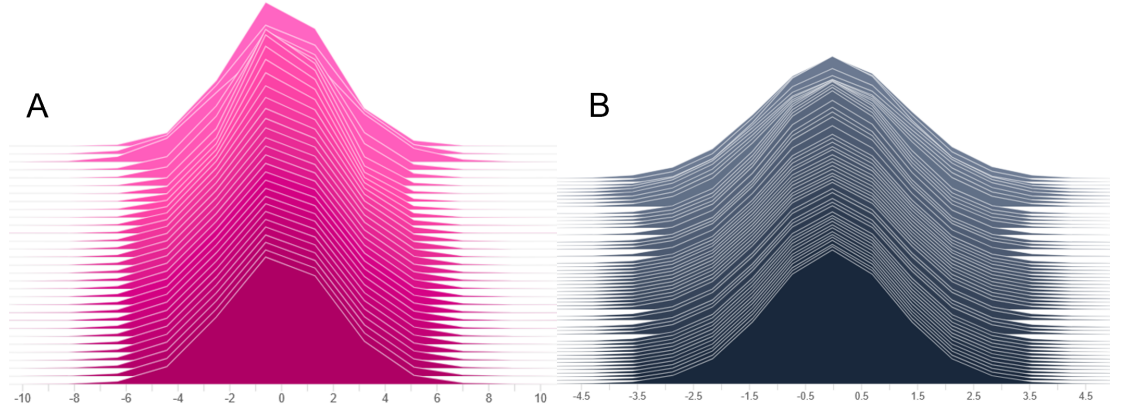


Figure 6. Activation levels of the final encoder layer of ConvNeXtV2-Base by epoch. (A) GCond is on the left. (B) The linear combination (Baseline) is on the right

Integration with Optimizers. Comparison of Integration Schemes with AdamW

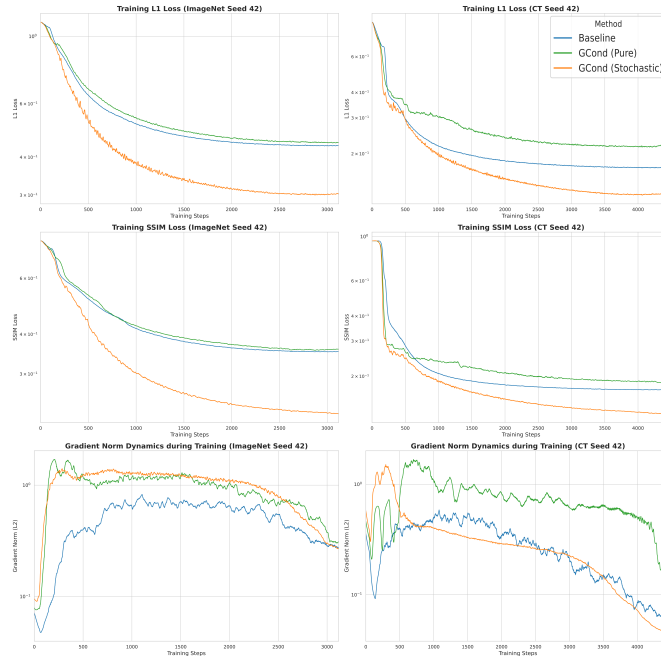


Figure 7. Comparison of convergence for L1 and SSIM losses, and L2-norms of gradients for the stochastic and pure GCond modes, and Baseline on both datasets during MobileNetV3-Small model training

The interaction between GCond and the AdamW optimizer was investigated using two schemes: Integrated: GCond performs the projection and EMA-smoothing of the gradient, while AdamW is used only for RMS-normalization ($\beta_1 = 0$). Separate (Pure): GCond performs only the projection, with its internal EMA-smoothing disabled. AdamW operates in its standard mode ($\beta_1 > 0, \beta_2 > 0$). The results showed a significant advantage for the integrated scheme. The key factor is the strict order of operations: when the adaptive denominator of AdamW operates on an already-agreed-upon and smoothed gradient vector, the update step becomes more stable. In the separate scheme, the internal momentum of AdamW attempts to smooth an already-corrected but still non-stationary sequence of gradients, leading to an overestimated variance and premature training stagnation.

Experiments with the Lion/LARS Optimizer

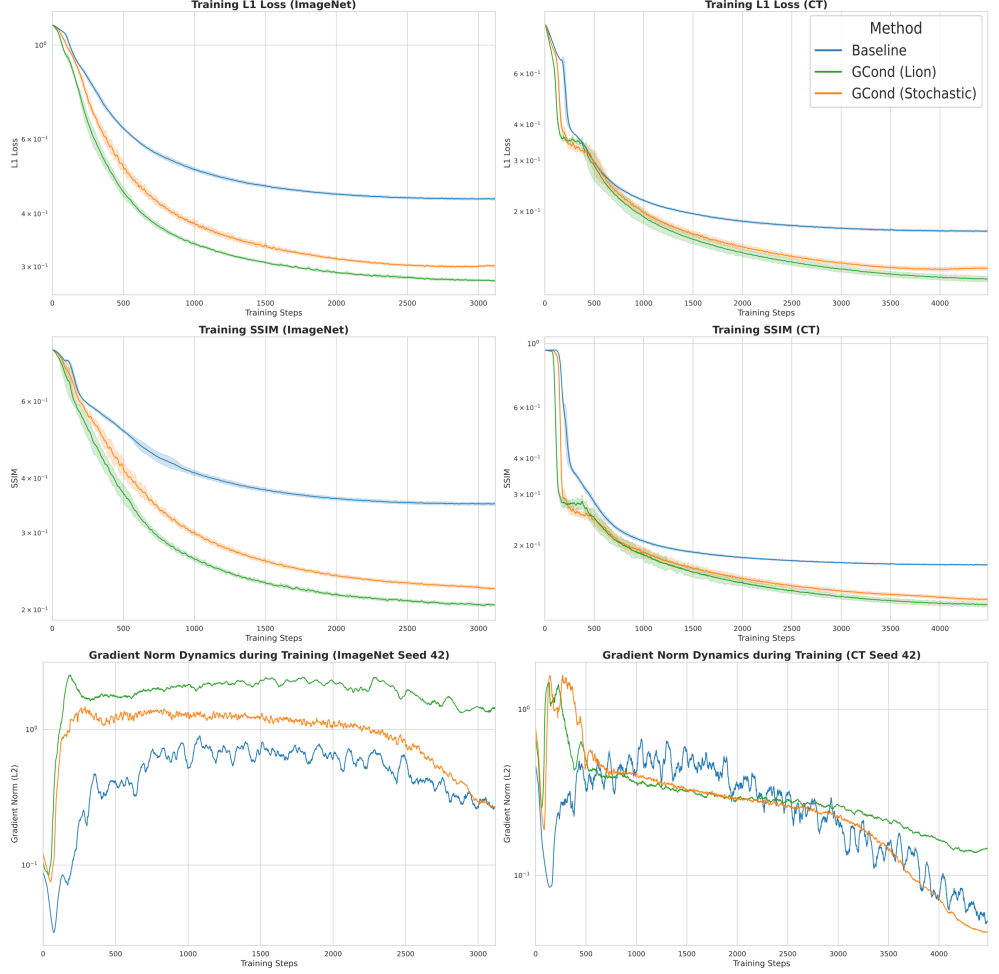


Figure 8. Comparison of convergence for L1 and SSIM losses, and L2-norms for the stochastic GCond mode and GCond with the Lion/LARS optimizer, and Baseline on both datasets during MobileNetV3-Small model training

The integrated GCond mode was tested with a hybrid optimizer combining principles from Lion and LARS: the update direction is given by $\text{sign}(m_t)$, where m_t is the smoothed momentum, and the magnitude is scaled by an adaptive learning rate (trust-ratio)

$$\frac{\|\mathbf{p}\|}{\|\mathbf{m}_t\|}$$

(where \mathbf{p} are the model weights). This approach combines the decisiveness of Lion, which ignores gradient magnitude to prevent getting stuck in narrow local minima, with the stabilizing normalization of LARS.

This resulted in a more confident loss reduction and convergence to a lower plateau compared to AdamW. Fig. 8 clearly shows that GCond with the Lion/LARS optimizer demonstrated a substantial reduction in L1 and SSIM losses, combined with better gradient L2-norms, compared to both the stochastic GCond mode using AdamW and the Baseline method. It is also worth noting that replacing AdamW with an optimizer that does not require storing second moments of the gradient, such as Lion, leads to a significant reduction in VRAM consumption, as it eliminates the need to store an additional copy of the model parameters. This is critically important for training large architectures. As shown by the validation curves in Fig. 9.

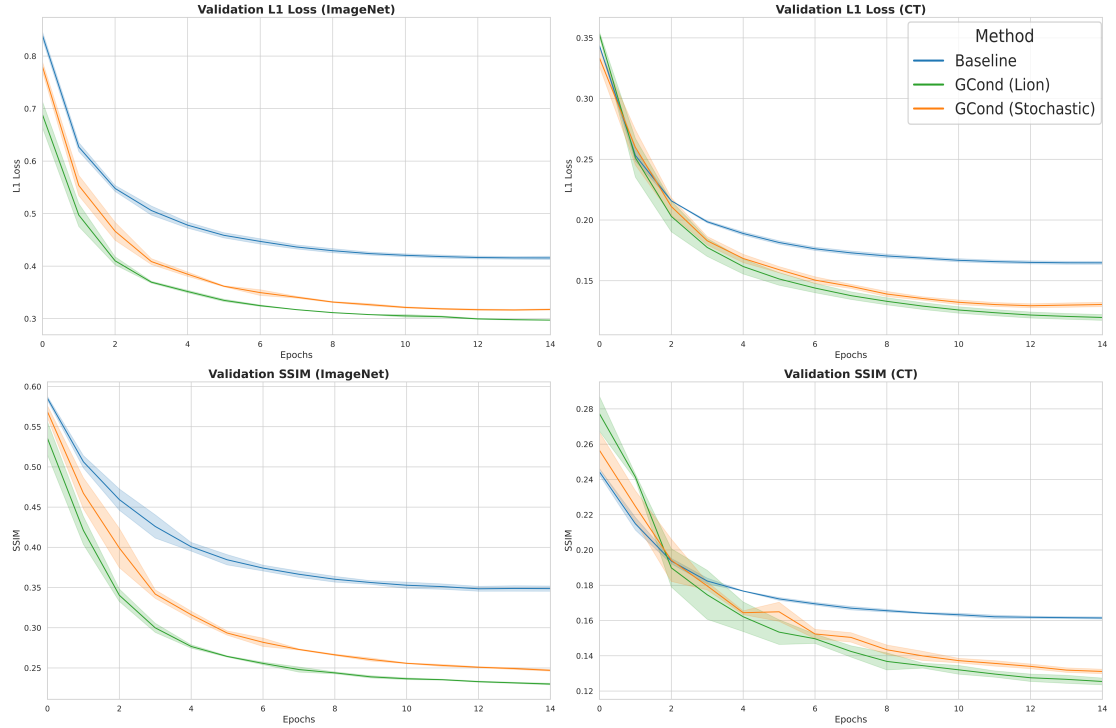


Figure 9. Validation of L1 and SSIM loss functions for the stochastic GCond mode and GCond with the Lion/LARS optimizer, and Baseline on both datasets during MobileNetV3-Small model training

It should be emphasized that a systematic comparison of all analyzed methods with the Lion and LARS optimizers was intentionally not conducted, and this result should be considered a promising direction for future research.

Visual Analysis of Reconstruction Quality

A qualitative comparison of results on the ImageNet validation set demonstrates that both the stochastic and, especially, the Lion-version of GCond provide visually more accurate and detailed reconstructions of masked images compared to the Baseline and other state-of-the-art methods Fig. 10. The improvements are particularly noticeable in the restoration of fine details, textures, and the preservation of the overall image structure.

The obtained results confirm the effectiveness of the proposed GCond approach in both quantitative metrics and the qualitative assessment of reconstruction outcomes, demonstrating its superiority over existing methods for resolving gradient conflicts in multi-task learning.

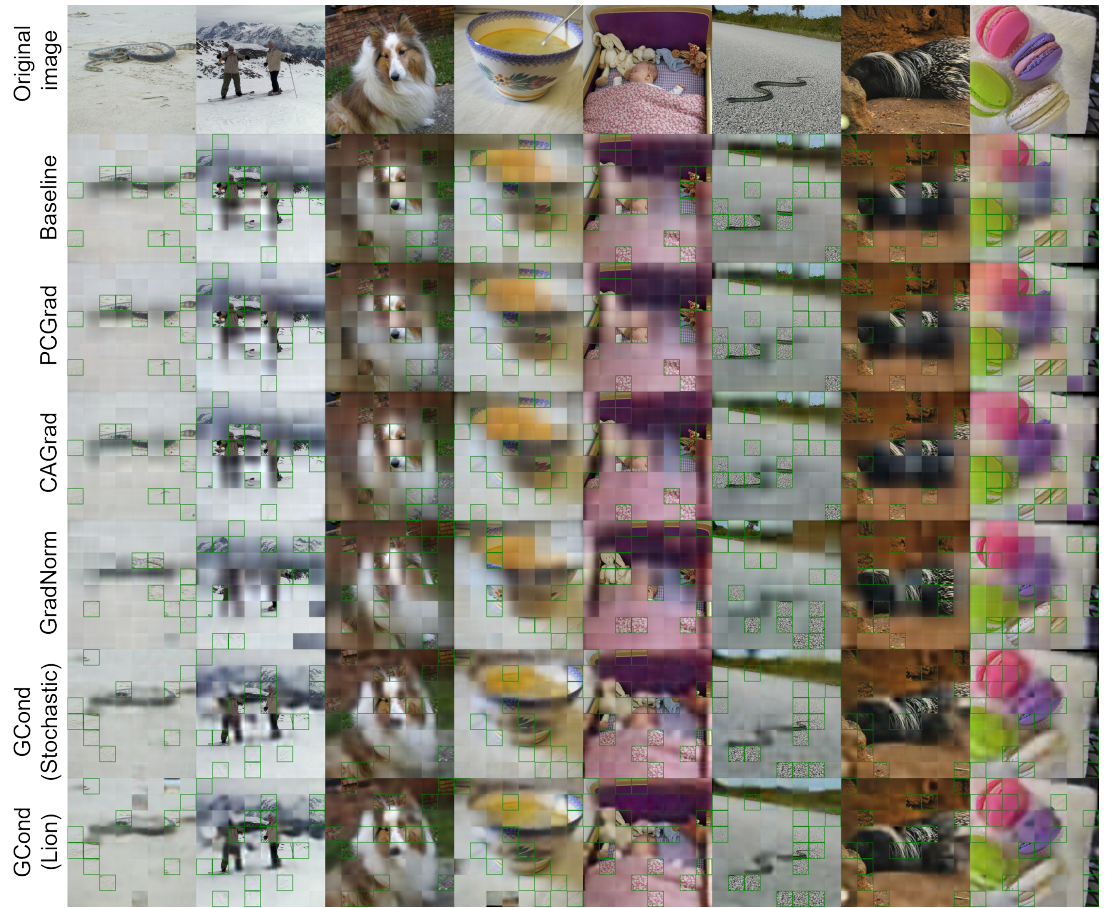


Figure 10. Comparison of image reconstructions. The cells highlighted in green were visible to the model.

DISCUSSION

Analysis of gradient dynamics revealed characteristic shortcomings of existing methods. GradNorm and PCGrad create significant sawtooth-like oscillations in amplitude, while CAGrad systematically over-suppresses the gradient norm. The reasons for this behavior lie in the nature of these algorithms. The core idea of GradNorm is to dynamically adjust loss weights to equalize the learning rates of different tasks by normalizing the norms of gradients passing through shared network layers, preventing one task from dominating others Chen et al. (2018). However, re-tuning GradNorm’s weights based on the instantaneous norms of a single shared layer provides a noisy proxy signal, especially under mixed-precision (AMP) and accumulation settings, leading to excessive corrections. PCGrad iteratively manipulates gradients by projecting the gradient of one task onto the normal plane of another’s when they conflict Yu et al. (2020). In doing so, PCGrad’s hard projections can nullify useful gradient components during a conflict, stochastically reducing the effective optimization step size. CAGrad extends the idea of PCGrad, seeking a single update vector that minimizes conflict with all tasks simultaneously Liu et al. (2021). However, CAGrad’s internal optimization problem often finds a convex combination with additional normalization, which reduces the gradient norm and can exacerbate underfitting. Thus, despite the theoretical elegance of existing gradient conflict resolution methods, our experiments show that their continuous and unconditional application can be counterproductive. In phases where gradients are nearly co-directional, applying these methods can remove useful shared components, slowing convergence. Furthermore, these methods do not consider the optimization history, making them vulnerable to short-term gradient oscillations. Against this backdrop, the simple summed gradient of the Baseline remains an unbiased, lower-variance estimate of the descent direction and therefore proves to be a more reliable solution when using a large effective batch size. In contrast, our comparative analysis demonstrates

the significant superiority of the proposed GCond method over existing conflict resolution techniques and the Baseline approach. This is because, unlike the aforementioned methods, GCond implements a multi-phase, adaptive strategy that does not apply corrections unnecessarily. It forms a single gradient with a high signal-to-noise ratio through a suite of complementary mechanisms. These include: the functional computation of individual task gradients while temporarily setting the model to `eval()` mode (disabling Dropout and using running statistics for BatchNorm); a smoothed projection with conflict angle remapping; a "winner-loser" arbitration mechanism based on stability relative to the previous step and EMAs of norms; and finally, EMA smoothing and bias correction before feeding the gradient to the optimizer. GCond's operation can be characterized by three distinct phases. The Initial Phase, where active projection correction is applied to quickly exit regions of strong conflict. This is followed by the Harmonious Descent Phase, where projections are automatically deactivated when gradients become co-directional ($\cos \theta \approx 1$), preventing excessive manipulation and accelerating learning. The final stage is the Plateau Navigation Phase. When learning slows, GCond detects the re-emergence of weak conflicts and reactivates its corrective mechanism, enabling it to find paths for further loss reduction where other methods stagnate. A key element of this approach is the hybrid arbitration, which considers not only the current geometry of the gradients but also their historical stability (similarity to the previous step) and relative strength when selecting a dominant task. This allows GCond to avoid unfavorable compromises and find an optimization trajectory that effectively improves both target metrics. As a result, GCond's trajectory exhibits more monotonic and less noisy behavior; destructive projections are mitigated smoothly, and the step direction is statistically grounded and virtually invariant to the scale of the layers.

Architectural Advantages

The development of the stochastic GCond mode is a significant methodological contribution, as it solves the critical problem of computational scalability while preserving optimization quality. The fact that the differences between the stochastic and exact modes are within the range of statistical noise Fig. 2 confirms the hypothesis that sparse gradient sampling is sufficient to form a statistically reliable estimate of conflicts when using large effective batch sizes. The primary advantage of GCond is its scalability on large models. We note that while any method could theoretically be rewritten using `torch.func` to partially reduce memory overhead, the superiority of our approach is not merely implementational. It stems from the symbiosis of gradient accumulation with a smooth, statistically-grounded conflict resolution logic. In contrast, an ablation study of a "GCond-as-PCGrad" variant (using hard projections) shows a noticeable degradation in quality and efficiency, although it still outperforms a naive PCGrad implementation with random projection order. While methods like PCGrad and CAGrad in their original implementations were unable to run on the ConvNeXt-Base architecture-as their computational complexity and memory requirements grow at least linearly with the number of tasks-GCond successfully processed up to 70 images per batch. This was achieved by sequentially computing gradients for specific tasks within dedicated accumulation windows without retaining the computation graph, making GCond an ideal solution for training large modern models and transformers under limited computational resources where memory is the bottleneck. Experiments with ConvNeXt-Base demonstrated not only quantitative improvements in metrics but also qualitative changes in model training. The nearly twofold expansion in the activation distribution of the final encoder layer from the very first epochs indicates the formation of richer, non-collapsing representations. We interpret this as a direct consequence of the high signal-to-noise ratio in the gradient and the conflict-resilient projection, which potentially enhances the model's generalization capability. Furthermore, GCond integrates exceptionally well with modern optimizers. The integration with Lion Chen et al. (2023), which determines the step direction via the sign operation, and LARS You et al. (2017), which adaptively scales the step magnitude, demonstrated superior results compared to the standard stochastic GCond mode with AdamW. The combination of Lion's decisiveness, which ignores gradient magnitude, with the stabilizing normalization of LARS creates a synergistic effect, ensuring a faster and more stable reduction in the loss function. This decomposition of tasks-geometry handled separately from step adaptation-maintains moderate orthogonality between tasks throughout training, allowing for continuous fine-grained adjustments that lead to better final solutions. The comparison between the "pure" GCond variant (without internal smoothing) and the standard integrated version highlighted the importance of the order of operations in adaptive optimization. The integrated scheme, where AdamW's adaptive denominator operates on an already-agreed-upon and smoothed gradient vector, provides significantly more stable update steps. This allows AdamW (with β_1 disabled to avoid redundant

momentum) to take large, consistent steps and sharply accelerates convergence. The even lower L1/SSIM losses achieved by replacing the optimizer with Lion confirm that the quality of the direction is more critical than its magnitude alone. Together, these factors explain the sharp reduction in L1 and SSIM for the GCond method on both datasets and the absence of the training trajectory noise characteristic of naive gradient conflict methods. This indicates the potential for further development of specialized optimizers for multi-task learning.

Analysis of Conflict Angle Dynamics

The curves of minimum cosine similarity show that GCond, particularly the Lion variant, quickly dampens early acute conflicts and transitions the multi-task dynamics into a stable "collinear" mode for most of the training trajectory Fig. 11. Sporadic late-stage activations represent brief, targeted projections just before the model's final fine-tuning. The stochastic mode without Lion also remains passive until the later stages; however, as the capacity of MobileNetV3-Small is exhausted and filter specialization increases, an "active competition for parameters" emerges. The minimum cosine similarity drops, and the arbitrator engages a soft projection with angle remapping to locally redistribute the task contributions.

This stability is explained by GCond's architecture. First, the hierarchy of conflict zones with non-linear angle remapping prevents hyper-correction during minor disagreements. Second, the arbitration based on "stability \times strength" criteria with dominance memory suppresses oscillations and cycles. Third, the EMA-norms in the stochastic mode and the corrected momentum with LARS-tuning in the Lion version equalize the scale of the directions. For comparison, PCGrad, by constantly performing pairwise orthogonalization, keeps the minimum cosines in the negative region, locking the system in a conflict mode and destroying the agreed-upon descent direction. This explains why GCond does not intervene for most of the training process but resolves conflicts in a targeted manner during the final stages, which correlates with the continued reduction in L1 and SSIM losses after all other compared methods have plateaued.

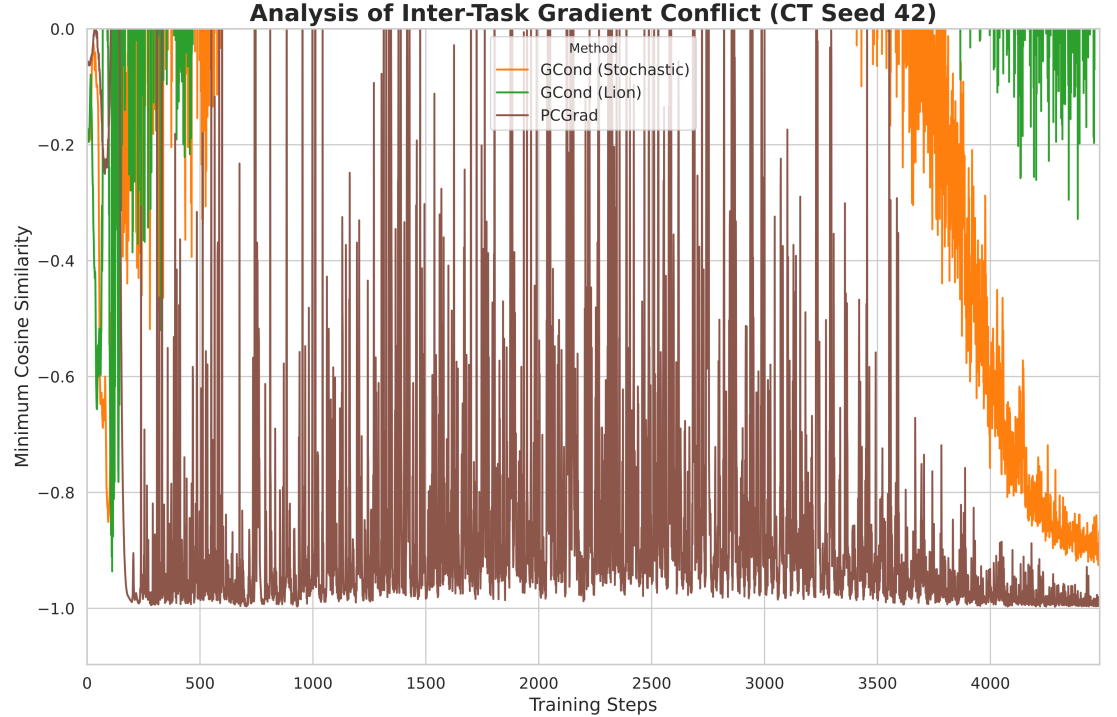


Figure 11. Cosine similarity of the most conflicting gradient pair at each step on the CT dataset

Analysis and Comparison with PCGrad

Given that GCond's design was inspired by PCGrad, a direct comparison was performed between the original PCGrad, a "GCond-as-PCGrad" ablation, and the standard stochastic GCond. The proposed

GCond module forms a unified gradient based on a global search for the most conflicting task pair, arbitration with a hybrid criterion (combining cosine stability to the previous step with relative norm strength), and a smooth projection with non-linear angle remapping, followed by EMA-smoothing with bias correction. As shown in Fig. 12, both GCond versions exhibit significantly less variance and an absence of sharp spikes, indicating a more stable update direction. In terms of minimum cosine similarity, the original PCGrad remains in a strong conflict mode (values near -1), whereas GCond quickly moves the loss pair out of the critical zone thanks to its arbitration and modular projection.

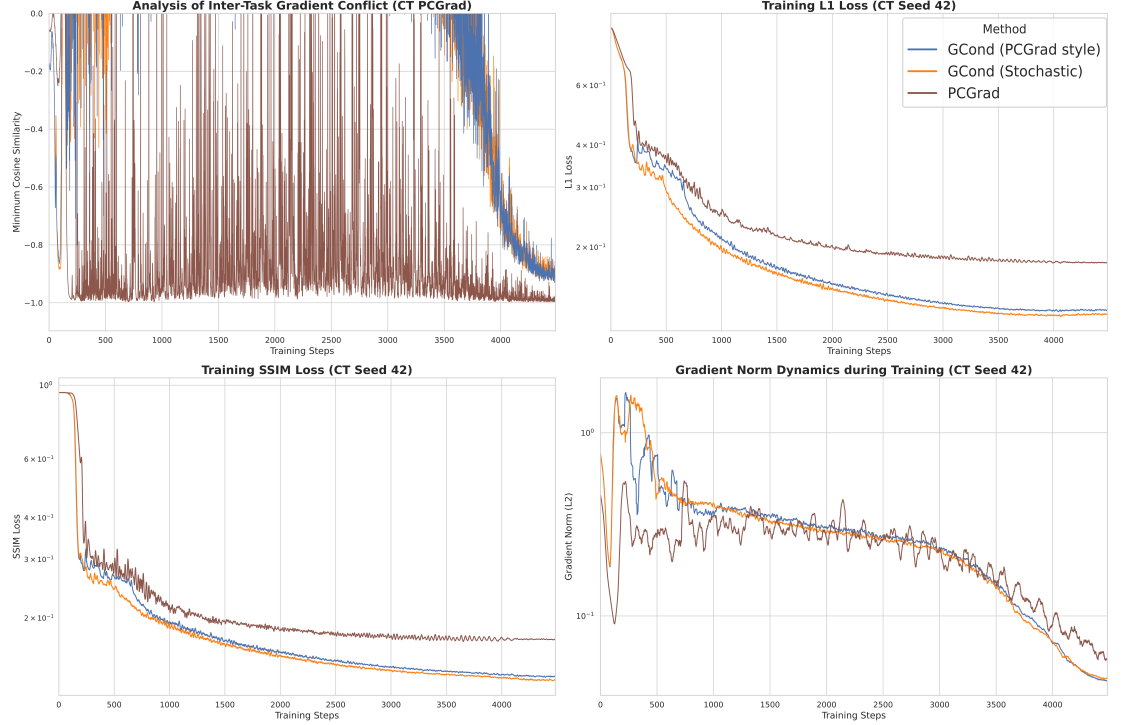


Figure 12. Cosine similarity of the most conflicting gradient pair at each step on the CT dataset and comparison of L1 and SSIM loss dynamics for PCGrad, ”GCond-as-PCGrad,” and stochastic GCond on the CT dataset

The L1 and SSIM loss curves of the methods coincide only in the early phase, after which PCGrad gets stuck in a ”tug-of-war” with pronounced oscillations, while GCond continues its monotonic descent. The quality and efficiency of the ” GCond-as-PCGrad” conductor are noticeably lower than the stochastic mode, although they remain superior to the naive PCGrad variant with random projections due to the global conflict assessment and symmetric projection. The full GCond mode, with its smooth function and EMA-smoothing, further reduces noise and establishes a more confident direction. As a result, the optimizer takes larger, more reliable steps, which resolves the inter-task conflict and leads to accelerated convergence for both loss functions.

Current Limitations

Several limitations should be considered when applying the proposed approach. GCond introduces hyperparameters-cosine similarity thresholds (-0.8, -0.5, 0.0) for its tiered conflict resolution strategy, along with weights for the arbitration criteria. Although these defaults proved robust across two different datasets, a systematic analysis of their sensitivity and the potential development of auto-tuning mechanisms are required. Another limitation is the reliance on large batch sizes. In this work, we intentionally focus on regimes with a large effective batch size, achieved through deep gradient accumulation, because GCond’s adaptive mechanisms depend on stable, low-variance estimates. Therefore, a direct comparison with state-of-the-art methods on classic MTL benchmarks (e.g., NYUv2, Cityscapes), where training is conducted with small batches and high gradient variance, would be methodologically inappropriate due to the differing computational paradigms. It should also be emphasized that GCond is not a universal

solution. In cases of persistent, nearly anti-parallel gradients (approaching 180°), the rigid "winner-takes-all" scheme could potentially impair convergence. In practice, it may be advisable to first align task weights using simpler loss functions before applying GCond with a large effective batch. The current implementation of GCond is tailored for PyTorch ≥ 2.0 and utilizes `torch.func.functional_call`, AMP/GradScaler, and optional DDP synchronization. Porting it to other frameworks or versions < 2.0 would require adapting these components.

Practical Implications

GCond presents a scalable solution for multi-task learning that can be easily integrated into existing PyTorch ≥ 2.0 -based deep learning frameworks without significant architectural changes. It can be incorporated as a "drop-in" component, as it operates on top of an existing gradient accumulation loop and writes the unified gradient vector directly to `p.grad`. This integration requires minimal code modifications and remains compatible with any optimizer and GradScaler (it is recommended to calculate momentum within the module). Moreover, GCond enables the formation of larger effective batches and the use of deeper architectures under the same hardware constraints, offering more efficient utilization of computational resources. Thus, the proposed GCond approach represents a practical solution for effectively resolving gradient conflicts in modern, large-scale multi-task learning models, opening new avenues for research in this field.

CONCLUSIONS

We have introduced Gradient Conductor (GCond), a novel approach to multi-task learning that addresses the fundamental limitations of existing gradient surgery methods. Through an "accumulate-then-resolve" paradigm and adaptive arbitration, GCond achieves superior performance while maintaining excellent scalability properties. Our experiments demonstrate significant improvements over state-of-the-art methods on both medical imaging and natural image datasets. The superiority of GCond stems from its core mechanism: a synergy of gradient accumulation and adaptive arbitration. This allows it to form a statistically reliable gradient direction by analyzing the optimization history and suppressing the noise of stochastic estimates. As a result, the final smoothed gradient enables modern optimizers like AdamW or Lion/LARS to take more confident steps, which translates directly into superior performance in both quantitative metrics and computational efficiency. A key feature is the ability to operate in a stochastic mode, providing an N-fold (where N is the number of loss functions) performance increase while maintaining optimization quality. Another advantage is its scalable architecture, which allows it to work with large models like ConvNeXt-Base where traditional methods in their original implementations are inapplicable. The high robustness of its hyperparameters and its successful integration with adaptive optimizers make GCond suitable for a wide class of deep learning tasks. This work opens up prospects for further research into the connection between conflict-resilient optimization and the generalization capabilities of neural networks, which may have fundamental implications for the advancement of MTL.

Funding Statement

The authors received no funding for this work.

Additional Information and Declarations

Acknowledgments The authors wish to thank The Cancer Imaging Archive (TCIA) and the Radiological Society of North America (RSNA) for providing the public datasets used in this study. The authors also acknowledge the use of Google's Gemini for assistance with the translation of the manuscript from Russian to English and for improving language and grammar. The authors reviewed and edited the text and bear full responsibility for the final content.

Competing Interests The authors declare there are no competing interests.

Author Contributions

- **Evgeny Alves Limarenko:** conceived and designed the experiments, performed the experiments, analyzed the data, performed the computation work, prepared figures and/or tables, and approved the final draft.

- **Anastasiia Alexandrovna Studenikina:** conceived and designed the experiments, analyzed the data, authored or reviewed drafts of the article, prepared figures and/or tables, and approved the final draft.

Data Availability The following information was supplied regarding data availability: The source code and experimental data for this study are available in a Zenodo repository (DOI: 10.5281/zenodo.17041808) and on GitHub (<https://github.com/AlevLab-dev/GCond>).

The datasets are available at:

- RSNA 2022 Cervical Spine Fracture Detection: <https://www.kaggle.com/competitions/rsna-2022-cervical-spine-fracture-detection/>
- RSNA Intracranial Hemorrhage Detection: <https://www.kaggle.com/competitions/rsna-intracranial-hemorrhage-detection>
- RADCURE from The Cancer Imaging Archive: <https://www.cancerimagingarchive.net/collection/radcure/>
- Benjamin paine Imagenet-1k-256x256: <https://huggingface.co/datasets/benjamin-paine/imagenet-1k-256x256>

Ethical Statement This study aims to develop a computationally efficient gradient conflict resolution method for multitasking learning, capable of working with modern large models while maintaining high optimization quality. The research utilizes only publicly available datasets (e.g., [RSNA 2022 Cervical Spine Fracture Detection]), ensuring compliance with their licensing requirements. No identifiable personal data was included, and no human participants were involved, thus exempting the study from requiring institutional ethical review. Throughout the study, strict adherence to academic ethical principles was maintained.

REFERENCES

- Borsani, T., Rosani, A., Nicosia, G., and Di Fatta, G. (2025). Gradient similarity surgery in multi-task deep learning. *ArXiv preprint*. arXiv:2506.06130.
- Chen, X., Liang, C., Huang, D., Real, E., Wang, K., Liu, Y., Le, Q. V., and et al. (2023). Symbolic discovery of optimization algorithms. *International Conference on Learning Representations (ICLR)*.
- Chen, Z., Badrinarayanan, V., Lee, C. Y., and Rabinovich, A. (2018). Gradnorm: Gradient normalization for adaptive loss balancing in deep multitask networks. In *International Conference on Machine Learning*, pages 794–803.
- Chen, Z., Ngiam, J., Huang, Y., Luong, T., Kretschmar, H., Chai, Y., and Anguelov, D. (2020). Just pick a sign: Optimizing deep multitask models with gradient sign dropout. *Advances in Neural Information Processing Systems*, 33:2039–2050.
- El Nahhas, O. S., Wölflein, G., Ligerio, M., Lenz, T., van Treeck, M., Khader, F., Kather, J. N., and et al. (2024). Joint multi-task learning improves weakly-supervised biomarker prediction in computational pathology. In *International Conference on Medical Image Computing and Computer-Assisted Intervention*, pages 254–262.
- Fifty, C., Amid, E., Zhao, Z., Yu, T., Anil, R., and Finn, C. (2021). Efficiently identifying task groupings for multi-task learning. *Advances in Neural Information Processing Systems*, 34:27503–27516.
- Flanders, A. E., Prevedello, L. M., Shih, G., Halabi, S. S., Kalpathy-Cramer, J., Ball, R., Mongan, J. T., Stein, A., Kitamura, F. C., Lungren, M. P., Choudhary, G., Cala, L., Coelho, L., Mogensen, M., Morón, F., Miller, E., Ikuta, I., Zohrabian, V., McDonnell, O., Lincoln, C., Shah, L., Joyner, D., Agarwal, A., Lee, R. K., Nath, J., and the RSNA-ASNR 2019 Brain Hemorrhage CT Annotators (2020). Construction of a machine learning dataset through collaboration: the rsna 2019 brain ct hemorrhage challenge. *Radiology: Artificial Intelligence*, 2(3):e190211.
- Golnari, A. and Diba, M. (2025). Adaptive real-time multi-loss function optimization using dynamic memory fusion framework: A case study on breast cancer segmentation. *ArXiv preprint*. arXiv:2410.19745.
- Jia, X., Song, S., Wei, H., Wang, Y., Rong, H., Zhou, F., Xie, L., Guo, Z., Yang, Y., Yu, L., Chen, T., Hu, G., Shi, S., and Chu, X. (2018). Highly scalable deep learning training system with mixed-precision: Training imagenet in four minutes. *ArXiv preprint*. arXiv:1807.11205.

- Kendall, A., Gal, Y., and Cipolla, R. (2018). Multi-task learning using uncertainty to weigh losses for scene geometry and semantics. In *Proceedings of the IEEE conference on computer vision and pattern recognition*, pages 7482–7491.
- Kim, J., Lee, Y., and Kang, P. (2024). A gradient accumulation method for dense retriever under memory constraint. *Advances in Neural Information Processing Systems*, 37:11765–11788.
- Lau, T. T.-K., Li, W., Xu, C., Liu, H., and Kolar, M. (2024). Communication-efficient adaptive batch size strategies for distributed local gradient methods. *ArXiv preprint*. arXiv:2406.13936.
- Lin, H. M., Colak, E., Richards, T., Kitamura, F. C., Prevedello, L. M., Talbott, J., Ball, R. L., Gumeler, E., Yeom, K. W., Hamghalam, M., Simpson, A. L., Strika, J., Bulja, D., Angkurawaranon, S., Pérez-Lara, A., Gómez-Alonso, M. I., Ortiz Jiménez, J., Peoples, J. J., Law, M., Dogan, H., and et al. (2023). The rsna cervical spine fracture ct dataset. *Radiology: Artificial Intelligence*, 5(5):e230034.
- Lin, X., Zhen, H. L., Li, Z., Zhang, Q. F., and Kwong, S. (2019). Pareto multi-task learning. *Advances in neural information processing systems*, 32.
- Liu, B., Feng, Y., Stone, P., and Liu, Q. (2023). Famo: Fast adaptive multitask optimization. *Advances in Neural Information Processing Systems*, 36:57226–57243.
- Liu, B., Liu, X., Jin, X., Stone, P., and Liu, Q. (2021). Conflict-averse gradient descent for multi-task learning. *Advances in Neural Information Processing Systems*, 34:18878–18890.
- Liu, Y., Li, A., Li, C., Yu, F., and Wang, B. (2025). Periodical moving average accelerates gradient accumulation for post-training. In *ICLR 2025*.
- Mang, C., Tahmasebimoradi, A., Danan, D., and Yagoubi, M. (2024). A dynamic weighted loss function for enhancing the performance of neural networks. In *16th World Congress on Computational Mechanics (WCCM)*.
- Navon, A., Shamsian, A., Achituve, I., Maron, H., Kawaguchi, K., Chechik, G., and Fetaya, E. (2022). Multi-task learning as a bargaining game. *ArXiv preprint*. arXiv:2202.01017.
- Peng, C., Xiao, T., Li, Z., Jiang, Y., Zhang, X., Jia, K., and Sun, J. (2018). Megdet: A large mini-batch object detector. In *Proceedings of the IEEE Conference on Computer Vision and Pattern Recognition*, pages 6181–6189.
- Piao, X., Synn, D., Park, J., and Kim, J. K. (2023). Enabling large batch size training for dnn models beyond the memory limit while maintaining performance. *IEEE Access*, 11:102981–102990.
- Rosenfeld, A. and Tsotsos, J. K. (2018). Incremental learning through deep adaptation. *IEEE transactions on pattern analysis and machine intelligence*, 42(3):651–663.
- Sener, O. and Koltun, V. (2018). Multi-task learning as multi-objective optimization. *Advances in neural information processing systems*, 31.
- Senushkin, D., Patakin, N., Kuznetsov, A., and Konushin, A. (2023). Independent component alignment for multi-task learning. In *Proceedings of the IEEE/CVF Conference on Computer Vision and Pattern Recognition*, pages 20083–20093.
- Shi, G., Li, Q., Zhang, W., Chen, J., and Wu, X.-M. (2023). Recon: Reducing conflicting gradients from the root for multi-task learning. *ArXiv preprint*. arXiv:2302.11289.
- Smith, S. L., Kindermans, P. J., Ying, C., and Le, Q. V. (2017). Don’t decay the learning rate, increase the batch size. *ArXiv preprint*. arXiv:1711.00489.
- Sun, Y., Xu, X., Li, J., Hu, X., Shi, Y., and Zeng, L.-L. (2025). Learning task-preferred inference routes for gradient de-conflict in multi-output dnns. *ArXiv preprint*. arXiv:2305.19844.
- Welch, M. L., Kim, S., Hope, A., Huang, S. H., Lu, Z., Marsilla, J., Kazmierski, M., Rey-McIntyre, K., Patel, T., O’Sullivan, B., Waldron, J., Kwan, J., Su, J., Soltan Ghoraie, L., Chan, H. B., Yip, K., Giuliani, M., Princess Margaret Head And Neck Site Group, Bratman, S., Tadic, T., and et al. (2023). Computed tomography images from large head and neck cohort. (radcure) (version 4) [dataset].
- Wu, F., Zhang, L., Sun, Y., Mo, Y., Nichols, T., and Papież, B. W. (2023). Multi-task cooperative learning via searching for flat minima. In *International Conference on Medical Image Computing and Computer-Assisted Intervention*, pages 171–181.
- You, Y., Gitman, I., and Ginsburg, B. (2017). Large batch training of convolutional networks. *ArXiv preprint*. arXiv:1708.03888.
- You, Y., Wang, Y., Zhang, H., Zhang, Z., Demmel, J., and Hsieh, C. J. (2020). The limit of the batch size. *ArXiv preprint*. arXiv:2006.08517.
- Yu, T., Kumar, S., Gupta, A., Levine, S., Hausman, K., and Finn, C. (2020). Gradient surgery for multi-task learning. *ArXiv preprint*. arXiv:2001.06782.

Zhang, Z., Shen, J., Cao, C., Dai, G., Zhou, S., Zhang, Q., Zhang, S., and Shutova, E. (2024). Proactive gradient conflict mitigation in multi-task learning: A sparse training perspective. *ArXiv preprint. arXiv:2411.18615*.

SUPPLEMENTARY MATERIALS

A EXPERIMENT HYPERPARAMETERS

To ensure the reproducibility of our results, this section details the complete set of hyperparameters used for each experimental condition. All experiments were conducted using three different random seeds (11, 42, 2025) to report mean performance and confidence intervals.

Constant Parameters

The following parameters were held constant across all training runs described in the main table below:

- **Model Architecture:**
 - Encoder: mobilenetv3_small1100
 - Decoder Embedding Dimension: 256
 - Decoder Depth (Transformer Blocks): 2
 - MAE Mask Ratio: 0.75
- **Data & Augmentation:**
 - Image Size: 256×256
 - Patch Size: 32×32
 - CT Dataset Mean / Std: 0.107961 / 0.173622
 - ImageNet Dataset Mean / Std: [0.485, 0.456, 0.406] / [0.229, 0.224, 0.225]
- **Training Framework:**
 - Epochs: 15
 - Total Batch Size: 256
 - Accumulation Steps: 24
 - Workers: 18
 - Gradient Clipping Norm: 50.0
- **LR Scheduler:**
 - Type: Linear Warmup + Cosine Annealing
 - Warmup Epochs: 2
 - Eta Minimum (Cosine): $1e-6$

Ablation Study and Baseline Parameters

The following table outlines the parameters that were varied across the different gradient management strategies. "N/A" indicates that a parameter is not applicable to the specified strategy.

Table 5. Hyperparameters for ablation studies and baseline comparisons with column borders.

Parameter Group	Parameter	Baseline	PCGrad	CAGrad	GradNorm	Conductor (Pure)	Conductor (Stochastic)	Conductor (Sequential)	Conductor (Lion)
General	Optimizer	AdamW							Lion/Lars ¹
	Learning Rate	2.0e-4							1.0e-5
	Weight Decay	0.05							N/A
	Adam β_1/β_2	0.9/0.95							N/A
	L_1 / SSIM λ	0.85/0.15			Dynamic	0.85/0.15			
Strategy-Specific	GradNorm α	N/A			1.5	N/A			
	GradNorm λ LR	N/A			1.0e-3	N/A			
Conductor: Core	return_raw_grad	N/A				True	False	False	False
	stochastic_accumulation	N/A				True	True	False	True
	use_smooth_logic	N/A				True			
	remap_power	N/A				2.0			
Conductor: Optimizer	use_lion	N/A				False	False	False	True
	momentum_beta (β_1)	N/A				0.0	0.9	0.9	0.9
	trust_ratio_coef (LR)	N/A				N/A			LR Sched. ²
	trust_ratio_clip	N/A				N/A			50.0
Conductor: Projection	projection_max_iters	N/A				3			
	norm_cap	N/A				None			
	conflict_thresholds	N/A				-0.8,-0.5,0			
Conductor: Arbitrator	dominance_window	N/A				0 - disabled			
	norm_ema_beta	N/A				0.95			
	tie_breaking_weights	N/A				(0.8, 0.2)			

¹ For the lion conductor mode runs, an external dummy SGD optimizer (lr=1.0, momentum=0.0) is used only to apply the final gradients computed by GradientConductor's internal optimizer. It does not perform any optimization logic itself.

² In Lion mode, the `trust_ratio_coef` is not a fixed value. Instead, it is dynamically set at each step to the current learning rate provided by the main learning rate scheduler, effectively making the scheduler control the magnitude of the Lion update.